UNIVERSAL WISER
PUBLISHER

Acetonitrile Synthesis via Ammoxidation: Mo/zeolites Catalysts Screening

Faouzi Ayari[*1], Emna Mannei[1,2], Esther Asedegbega-Nieto[3], Mourad Mhamdi[2,4], Gérard Delahay[5]

[1]Laboratory of chemical, galenic and pharmacological development of drugs, Faculty de Pharmacy of Monastir, University of Monastir, Monastir, Tunisia
[2]Material chemistry and catalysis laboratory, Faculty of Sciences of Tunis, University of Tunis El Manar, Tunis, Tunisia
[3]Department of inorganic and technical chemistry, Faculty of Sciences, The National Distance Education University, Madrid, Spain
[4]Higher institute of medical technologies of Tunis, University of Tunis El Manar, Tunis, Tunisia
[5]CNRS–UM–ENSCM–MACS, Charles Gerhardt Institute in Montpellier, Montpellier, France
E-mail: faouzi.ayari@fst.utm.tn

Abstract: Mo/zeolites catalysts were investigated in ethane and ethylene ammoxidation into acetonitrile. The catalysts were prepared either in solid-solid or liquid-solid interface after varying different parameters. The stabilization of Mo species upon the exchange is dependent on the hydrophilic/hydrophobic character of the zeolite and the type of Mo precursor. In fact, zeolites with low Si/Al molar ratios should be avoided due to their higher dehydration enthalpy values (Δ_{dehyd}.H). On the other hand, the use of $MoOCl_4$, $Mo(CO)_6$ and $MoCl_3$ precursors and zeolites with high Si/Al ratios led to inefficient $[Mo_7O_{24}]^{6-}$ species and amorphous MoO_3 which catalyzes the combustion reaction. Nevertheless, the use of $MoCl_5$, MoO_3 and $MoO_2(C_5H_7O_2)_2$ led to promising activities. In catalysis, $[MoO_4]^{2-}$ species are required to activate C_2H_6 into C_2H_4, while $[Mo_xO3_{x+1}]^{2-}$ (x =1, 2) species catalyze the ammoniation of C_2H_4 and the ethylamine dehydrogenation into CH_3CN. Interestingly, active catalysts could be obtained by humid impregnation and a simultaneous oxidative treatment. Such a treatment improves the dispersion state of crystalline MoO_3, which activate ethane molecules. It is judicious to perform C_2H_6 oxidative dehydrogenation before ammoxidation since the interference between the different investigated parameters could be noted.

***Keywords*:** Offretite, Ferrierite, Dehydration Enthalpy, Band Gap, MoO_3

1. Introduction

Will the world have enough ethane?

According to the statistics, 80% of the global production of C_2H_6 comes from 10 nations. However, ethane is difficult to transport and ~660 Trillion BTU of this hydrocarbon is either rejected in the natural gas or flared, leading to a waste of valuable resources[1, 2]. Fortunately, efforts were consented in the conversion of ethane to liquid hydrocarbons inside the natural gas deposits. Compared with ethane, ethylene is easier to convert into valuables liquids such as nitriles and therefore, the activation of C_2H_6 is a crucial step in the ethane-to-liquids technology.

Our group[3,4,5] has reported Mo/zeolites as efficient catalysts for ethane ammoxidation (Eq. 1) into acetonitrile (AN). The reaction in Eq. (1) is the sum of Eqs. (2), (3) and (4)[6].

$$C_2H_6 + NH_3 + 1.5O_2 \rightarrow CH_3CN + 3H_2O \quad (1)$$

$$C_2H_6 + 0.5O_2 \rightarrow C_2H_4 + H_2O \quad (2)$$

$$C_2H_4 + NH_3 \leftrightarrow CH_3CH_2NH_2 \quad (3)$$

$$CH_3CH_2NH_2 + O_2 \rightarrow CH_3CN + 2H_2O \quad (4)$$

However, ethylene ammoxidation (Eq. 5) is the sum of Eqs. (3) and (4) and, therefore, C_2H_4 is an intermediate during C_2H_6 ammoxidation[6].

DOI: https://doi.org/10.37256/fce.112020117.16-30

$$C_2H_4 + NH_3 + O_2 \rightarrow CH_3CN + 2H_2O \quad (5)$$

The manufacture of acetonitrile via ammoxidation has attracted the attention of scientists till date[5,7]. In fact, AN is particularly used as electrolyte in dye-sensitized solar cells[8] (dipole moment ~3.44 Debye[9]). Given the fact that AN is produced as a by-product during acrylonitrile manufacture, the growing demand for acrylonitrile products has led to a severe AN shortage mainly in the pharmaceutical industry[10]. However, the unexpected AN shortages can offer the opportunity for scientists to develop novel C_2H_6 ammoxidation catalysts[11,12].

The aim of this work is to study C_2H_6 and C_2H_4 ammoxidation into acetonitrile over Mo/zeolites catalysts. We performed a general screening of numerous catalysts issued from different zeolites' structure, Mo precursors, Si/Al molar ratio and Mo wt. % in order to optimize the adequate preparation parameters. Simultaneously, different characterization techniques have been used to study the physicochemical properties of the prepared solids.

2. Materials and Methods

2.1 Catalysts preparation

The samples were prepared by solid-state ion exchange (SSIE), which consists on grinding the zeolite and the Mo salt before being heated under a carrier gas from 30 to 500°C (2°C min^{-1}) and then kept isothermally for 12h at 500°C. Several reference solids were prepared either by SSIE or impregnation (Imp). The later method consists on mixing the zeolite with an aqueous solution containing the desired quantity of Mo precursor. For this purpose, the precursor was dispersed in a small quantity of water using sonication and, after the impregnation of the zeolite support, the resulting slurry was dried in oven at 100°C overnight before being treated under carrier gas for 12h at 500°C. More details are available in Tables 1 and S1.

Table 1. List of the prepared solids

No	Sample	Zeolite	Si/Al	Precursor	Treatment gas	Mo wt. %
		Solid–state ion exchange				
I	Mo–OFF	H–OFF	4	$MoCl_3$	He	9
II	Mo–FER	NH_4^+–FER	10	$MoCl_3$	He	9
III	Z26($MoCl_3$)	NH_4^+–ZSM-5	26	$MoCl_3$	He	6
IV	Z15($MoCl_3$)	H^+–ZSM-5	15	$MoCl_3$	He	9
V	MOR($MoCl_3$)	NH_4^+–MOR	10	$MoCl_3$	He	9
VI	BEA($MoCl_3$)	NH_4^+–BEA	12.5	$MoCl_3$	He	9
VII	Z26($MoOCl_4$)	NH_4^+–ZSM-5	26	$MoOCl_4$	He	6
VIII	Z26($MoCl_5$)	NH_4^+–ZSM-5	26	$MoCl_5$	He	6
IX	Z26(MoCO)*	NH_4^+–ZSM-5	26	$Mo(CO)_6$	He	6
X	Z26(MoAcac)	NH_4^+–ZSM-5	26	$MoO_2(C_5H_7O_2)_2$	He	6
XI	Z26(MoO_3)6%He	NH_4^+–ZSM-5	26	MoO_3	He	6
XII	BEA(MoO_3)	NH_4^+–BEA	12.5	MoO_3	He	6
XIIII	BEA(MoAcac)	NH_4^+–BEA	12.5	$MoO_2(C_5H_7O_2)_2$	He	6
XIV	BEA(MoCO)	NH_4^+–BEA	12.5	$Mo(CO)_6$	He	6
XV	BEA($MoCl_5$)	NH_4^+–BEA	12.5	$MoCl_5$	He	6
XVI	BEA($MoOCl_4$)	NH_4^+–BEA	12.5	$MoOCl_4$	He	6
XVII	BEA(Mo_7O_{24})	NH_4^+–BEA	12.5	$(NH_4)_6Mo_7O_{24}$	He	6
		Reference materials				
XVIII	Z26(MoO_3)10%He	NH_4^+–ZSM-5	26	MoO_3	He	10
XIX	Z140(MoO_3)6%He	NH_4^+–ZSM-5	140	MoO_3	He	6
XX	Z15(MoO_3)Imp2%	H^+–ZSM-5	15	MoO_3	O_2	2
XXI	Z15(MoO_3)Imp4%	H^+–ZSM-5	15	MoO_3	O_2	4
XXII	Z40(MoO_3)Imp2%	H^+–ZSM-5	40	MoO_3	O_2	2
XXIII	Z40(MoO_3)Imp4%	H^+–ZSM-5	40	MoO_3	O_2	4
XXIV	Z26(MoO_3)6%O_2	NH_4^+–ZSM-5	26	MoO_3	O_2	6
XXV	Z140(MoO_3)6%He	NH_4^+–ZSM-5	140	MoO_3	O_2	6

***See ref. [5]**

2.2 Catalytic tests and characterization techniques

Details about catalytic tests are available in the supplementary information section (p. S1). The chemical analyses have been performed by inductively coupled plasma (ICP) and energy dispersive X-ray (EDX).

Textural, structural and morphological studies have been performed by N_2 physisorption, X-ray diffraction (XRD), scanning electron microscopy (SEM) and transmission electron microscopy (TEM). The metal oxidation states were studied by X-ray photoelectron and UV/Vis diffuse reflectance spectroscopies (XPS and DRS). The redox features were investigated by temperature programmed reduction under hydrogen atmosphere (H_2-TPR), while the acidity was studied by ammonia thermo-desorption (NH_3-TPD) and diffuse reflectance infrared Fourier transform spectroscopy (DRIFTS).

3. Results

3.1 Catalytic behaviour of Mo containing catalysts

3.1.1 OFF, FER and MFI issued solids

The catalytic behaviour of the prepared solids is compiled in Tables S2-S4. Mo-OFF and Mo-FER catalysts exhibited low activities due to their particular structures and the nature of stabilized Mo species.

The catalysts No III-VI exhibited diverse catalytic activities. At 7% of ethane conversion, Z26($MoCl_3$) led to the highest AN selectivity at 500°C (49 %, vs. 4% for the inactive MOR($MoCl_3$) solid). In particular, BEA($MoCl_3$) led to the highest activity and selectivity toward ethylene(respectively 0.40 $\mu mols^{-1}g^{-1}$ and 17 % vs. 0.20 $\mu mols^{-1}g^{-1}$ and 10 % for Z15($MoCl_3$) at 500°C).

At 6% of ethylene conversion, MOR($MoCl_3$) exhibited the lowest AN selectivity, while Z26($MoCl_3$) exhibited the highest activity at 500°C (13.70 $\mu mols^{-1}g^{-1}$ vs. 11.40 and 6.70 $\mu mols^{-1}g^{-1}$ for Z15($MoCl_3$) and BEA($MoCl_3$), respectively).

Given the fact that ZSM-5 zeolite (Si/Al = 26) led to the best catalytic results, we used this support to introduce Mo at different oxidation states (Mo^{VI}, Mo^{V} and metallic Mo) as they play a crucial role in oxidation and hydrogenation reactions[13].

The catalytic activities obtained in ethane ammoxidation (Table S2) revealed that Z26($Mo^{VI}OCl_4$) and Z26(Mo^{VI}Acac) are poorly active solids (AN activity: 0.30 and 0.40 $\mu mols^{-1}g^{-1}$, respectively, at 500°C) if compared with Z26($Mo^{V}Cl_5$). On the other hand, the use of Mo in its lowest and highest oxidation states (i.e. by using, respectively, $Mo(CO)_6$ and MoO_3 precursors) led to promising catalytic properties (0.90 and 1.20 $\mu mols^{-1}g^{-1}$ of AN activity, respectively, at 500°C).

In ethylene ammoxidation, the situation is different. As refers to the solids obtained from Cl-containing precursors, Z26($MoCl_5$) exhibited the highest activity, while the activity of Z26($MoCl_3$) and Z26($MoOCl_4$) catalysts is quasi-similar at 500°C (Table S3). However, the use of MoO_3 at different Mo contents led to noticeable divergence in the activities over Z26(MoO_3)6%He and Z26(MoO_3)10%He (8.90 and 26.50 $\mu mols^{-1}g^{-1}$, respectively, Tables S3 and S4).

Concerning the effect of Mo oxidation state, the data compiled in Table S3 indicate that the catalyst obtained from $Mo^{VI}O_2(C_5H_7O_2)_2$ is poorly active if compared with Z26(MoCO) (respectively 5.40 and 20.90 $\mu mols^{-1}g^{-1}$ of AN activity at 500°C). Nevertheless, by varying Si/Al ratio (while maintaining Mo wt. % constant), we noticed that increasing the ratio value decreases the AN activity (8.90 to 5.60 $\mu mols^{-1}g^{-1}$, respectively, for Z26(MoO_3)6%He and Z140(MoO_3)6%He, Tables S3 and S4).

Apparently, the Si/Al ratio is another parameter to be considered during the preparation of ammoxidation catalysts. In line with this, the effect of both acidity (i.e. Si/Al ratio) and Mo wt. % was studied in ethylene ammoxidation over Z15(MoO_3)Imp2%, Z15(MoO_3)Imp4%, Z40(MoO_3)Imp2% and Z40(MoO_3)Imp4%. The obtained results indicate that Z15(MoO_3)Imp4% led to 100 % of selectivity toward AN at 20% of ethylene conversion (Table S4). However, with the same Mo amount (4 wt. %), the increase in Si/Al ratio does not affect the selectivity, while the activity was declined.

3.1.2 BEA issued solids

Among the catalysts issued from BEA zeolite (No XII-XVII), BEA($MoOCl_4$) was found to be less-active than BEA(MoAcac) in C_2H_6 ammoxidation at 500°C. On the other hand, both pairs of catalysts, i.e. BEA(MoO_3)/BEA(MoCO) and BEA($MoCl_5$)/BEA(Mo_7O_{24}) exhibited similar AN activity values (Table S2).

In ethylene ammoxidation, the difference in the catalytic properties at 500°C is obvious (Table S3). In effect, BEA(MoO_3) and BEA(MoAcac) exhibited the highest AN activities (19.30 and 18.10 $\mu mols^{-1}g^{-1}$, respectively), while BEA($MoCl_5$) and BEA($MoOCl_4$) are less-active (9.20 and 9.50 $\mu mols^{-1}g^{-1}$, respectively). Nonetheless, BEA(MoCO) and BEA(Mo_7O_{24}) exhibited intermediate AN activity values (15.20 and 12.70 $\mu mols^{-1}g^{-1}$, respectively).

3.2 Characterization of Mo containing solids

3.2.1 OFF and FER issued solids

Table S5 summarises the chemical composition of the solids No I and II as well as their exploitable textural properties. The recorded SBET values are too low to be accurately interpreted, in particular for H^+-OFF, $NH4^+$-FER and Mo-FER samples. In a similar way, and due to the presence of Na^+ and K^+, low textural data were obtained with zeolite A[14] and

offretite[15]. Nevertheless, in the case of Mo-OFF solid, the S_{BET} value was improved (108 m^2g^{-1}) owing to the loss of cations upon SSIE.

The data compiled in Table S5 revealed that the $(Mo/Al)_{XPS}$ ratios for the solids No I and II exceed those determined by ICP, which indicates that Mo occupied the surface. Interestingly, the $(Mo/Al)_{XPS}$ ratio determined for Mo-FER solid is quite high (8.5 vs. 4 for Mo-OFF), evidencing that the surface contains a significant amount of metal. Effectively, the SEM analysis revealed the presence of small particles of NH_4^+-FER zeolite (Fig. S1), which indicates that the external surface is well–developed.

The XP spectrum of Mo-OFF solid (Fig. 1A) indicated the presence of MoO_3 and MoO_2[16]. The presence of such moieties was confirmed by TPR (Fig. S2), which revealed two reduction peaks at 608 and 816°C ascribed, respectively, to the processes described in (Eq. 6) and (Eq. 7)[17, 18].

$$MoO_3 + H_2 \rightarrow MoO_2 + H_2O \quad (6)$$

$$MoO_2 + 2H_2 \rightarrow Mo + 2H_2O \quad (7)$$

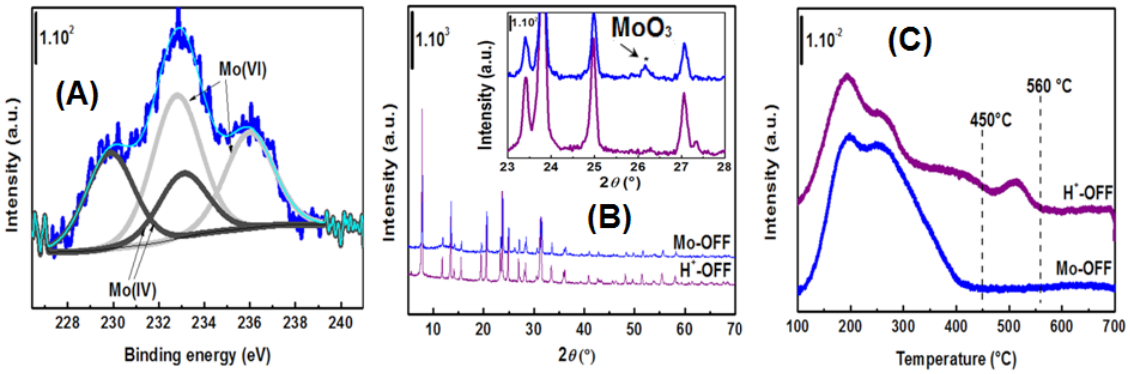

Figure 1. (A) XP spectrum of Mo-OFF solid (B) XRD patterns of Mo-OFF solid and the corresponding support, and (C) NH3-TPD profiles of Mo-OFF and H+-OFF solids

The TEM images of Mo-OFF (Fig. S3) showed tubular–like silicate crystals and small oxide particles. At the same time, the XRD pattern of this sample (Fig. 1B) showed a diffraction line ascribed to crystalline MoO_3. On the other hand, the EDX analysis revealed, besides $_{19}K$ (5-7 wt. %), the homogenous dispersion of Mo at the surface (~7 wt. %, Table S6).

The acidity was studied by NH_3–TPD. The profiles of Mo-OFF and H^+-OFF solids (Fig. 1C) highlighted a noticeable difference. In fact, between 450 and 560°C, the zeolite desorbed NH_3 from strong acidic sites situated inside the internal cages. However, after SSIE, this peak disappeared as the internal cages of offretite become inaccessible to NH_3.

The nature of Mo species stabilized over Mo–OFF solid was estimated by the band gap energy values determined by DRS. The spectrum representing $[F(R\infty)\times hv]^{0.5}$ vs. hv[4,5] is illustrated in Fig. 2.

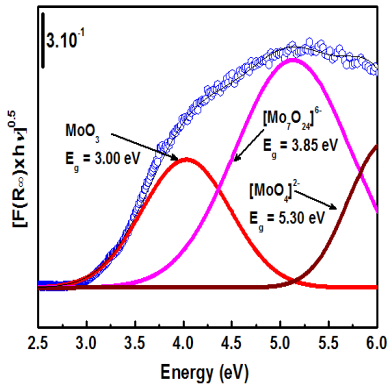

Figure 2. Optical absorption spectrum of Mo-OFF solid. F(R∞) is the Schuster-Kubelka-Munk function, while hv is the photon energy[4,5]. Eg: Edge energy

The deconvolution of Mo-OFF spectrum revealed three $O^{2-}\rightarrow Mo^{6+}$ charge transfer bands assigned to MoO_3 (E_g = 3.00

eV), $[Mo_7O2_4]^{6-}$ (E_g = 3.85 eV) and $[MoO_4]^{2-}$ (Eg = 5.30 eV)[4, 5]. In this spectrum, we were not able to detect the presence of $[Mo_2O_7]^{2-}$ species characterized by a band between 3.85 and 5.3 eV.

On comparing with the starting material, NH_4^+-FER zeolite, the SSIE of this zeolite with $MoCl_3$ decreased the intensity of the silanol DRIFTS's band (at 3735 cm^{-1}, Fig. 3A). On the other hand, the XPS results (Table S5) indicate that a significant fraction of Mo is present at the surface in the form of crystalline MoO_3 (Figs. 3B and 3C).

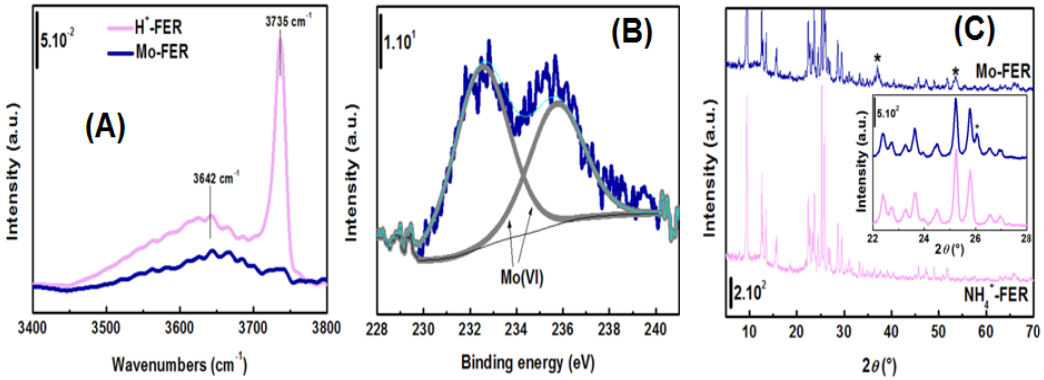

Figure 3. (A) DRIFTS spectra of H+-FER and Mo-FER solids, (B) XP spectrum of Mo-FER solid, and (C) XRD patterns of Mo-FER solid and the corresponding support

It is important to note that the intensity of the band ascribed to silanol groups in Fig. 3A is very high, which corroborates the fact that the external area of NH_4^+-FER is well-developed (Fig. S1).

3.2.2 MFI, MOR and BEA zeolites exchanged with $MoCl_3$

The solids No III-VI were characterized in our previous work[19]. However, using DRS, we revealed in this study that these solids stabilized MoO_3 and $[MoO_4]^{2-}$ species (Figs. S4A-D). In particular, MOR support extended the formation of MoO_3 due to its particular structure[19], while MFI and BEA issued solids loaded with small aggregates of MoO_3 (see XRD results in[19]). Interestingly, $[Mo_2O_7]^{2-}$ species were detected only over MFI solids (Figs. S4A,B and DRS results in[19]), while the formation of heptamers was inhibited over Z26($MoCl_3$) (Fig. 4SB).

Our experience with the mechanistic study of SSIE has shown that the nature of Mo species depended on the hydration state of the zeolite. For this purpose, we determined the dehydration enthalpies ($\Delta_{dehyd.}H$) of the different zeolites (Table 2) according to Eq. (8)[20].

$$\Delta_{dehyd.}H = \frac{Al}{Si} \times e^{\left[5.491-(4.674\times\left\langle\frac{Al}{Si+Al}\right\rangle)\right]} \qquad (8)$$

Table 2. Dehydration enthalpy ($\Delta_{dehyd.}H$) of the zeolites used in this study

Zeolite	Si/Al (mol/mol)	$\Delta_{dehyd.}H^+$ (kJ mol^{-1})
H^+–OFF	3.34	24.73
NH_4^+–FER	9.11	16.77
H^+–ZSM-5 (Si/Al=15)	15.66	11.70
NH_4^+–ZSM-5 (Si/Al=26)	27.01	7.60
NH_4^+–BEA	12.21	13.94
NH_4^+–MOR	6.85	19.52

According to Table 2, ZSM-5 zeolite (Si/Al = 26) exhibited the lowest $\Delta_{dehyd.}H$ value, while the offretite (Si/Al = 3.34) undergoes the highest one. Seemingly, one and bi–dimensional zeolites were hardly dehydrated if compared with 3D-ones (MFI and BEA).

3.2.3 NH_4^+-ZSM-5 (26) exchanged with $MoOCl_4$, $MoCl_5$, $Mo(CO)_6$, MoO_3 and $MoO_2(C_5H_7O_2)_2$

This category of solids was almost characterized in our earlier works[3-5, 18]. However, we represent in Table 3 the data relative to the solids No VII-XI and III for comparison purpose.

Table 3. DZSM-5 (26) issued solids: Textural and chemical analyses results

Sample	S_{BET}/S_{micro}	V_p/V_{micro}	Si/Al		Mo wt. %		Mo wt. loss*	
	(m^2g^{-1})	($cm^3\ g^{-1}$)	ICP[a]	EDX[a]	ICP	EDX	ICP	EDX
NH_4^+–ZSM-5 (26)	367/291	0.21/0.13	27.01	28.34	–	–	–	–
Z26($MoOCl_4$)	–	–	–	26.17	–	5.14	–	14
Z26($MoCl_5$)	354/232	0.19/0.10	24.46	27.62	4.15	3.06	31	49
Z26(MoCO)	269/182	0.17/0.08	25.15	25.67	1.86	3.00	69	50
Z26(MoO_3)6%He	340/223	0.21/0.10	25.05	22.44	3.67	–	39	–
Z26(MoAcac)	305/205	0.18/0.09	24.85	24.47	3.88	5.69	35	10
Z26($MoCl_3$)	343/230	0.19/0.10	26.96	27.56	4.54	4.90	24	18

* $[(Mo_{theoret.}- Mo_{ICP\ or\ EDX})/Mo_{theoret.}] \times 100$, [a] mol/mol

According to Table 3, the solids exhibited low Mo wt. % if compared with the theoretical value (6 wt. %). This behaviour would be originated from the evaporation of Mo intermediates during the SSIE procedure[5]. In particular, Z26(MoCO) solid exhibited a high metal loss ascribed to the evaporation of the precursor during the exchange[21]. On the other hand, the low SBET and porosity of this solid would be originated from the presence of oxide particles at the near–surface[5].

The DRS results are compiled in Table 4. The amount and the percentage of each Mo moiety were determined by Eq. (9) upon the deconvolution of the optical spectra (see Fig. S5) and using the absorption coefficients (k) relative to MoO_3, $[Mo_7O_{24}]^{6-}$, $[Mo_2O_7]^{2-}$ and $[MoO_4]^{2-}$ determined[4].

$$C_{Mo}=A_{Mo}\times k_{Mo} \quad (9)$$

Here, C_{Mo} is the concentration of the Mo specie ($molg^{-1}$), A stands for the band's area (*a.u.*) depicted in Table S7 and k for the absorption coefficient.

Table 4. Amount and molar fraction of each Mo moiety over ZSM-5 (Si/Al = 26) issued solids

Sample	Amount Mo moieties ($\mu molg^{-1}$) and the corresponding molar fraction (%, value between brackets)				
	$[MoO_4]^{2-}$	$[Mo_2O_7]^{2-}$	$[Mo_7O_{24}]^{6-}$	MoO_3	Mo amount ($molg^{-1}$)
Z26($MoCl_5$)	–	78.9 (33)	–	158 (67)	3.20×10^{-4}
Z26($MoCl_3$)	344 (67)	53 (10)	–	115 (23)	5.11×10^{-4}
Z26(MoCO)	–	75 (36)	5.4	126.8 (61)	3.13×10^{-4}
Z26(MoO_3)6%He	ND*	28 (8.5)	5.11	10.5 (3.2)	–
Z26($MoOCl_4$)	340 (64)	80 (15)	6.5	108 (20)	5.36×10^{-4}
Z26(MoAcac)	418 (70)	50 (8)	4.3	121 (20)	5.93×10^{-4}

*The band in ref. [18] is not credulous

Whatever the oxidation state of Mo in the used precursor, the DRS results indicate that SSIE stabilizes Mo^{VI} species.

The data compiled in Table 4 indicate that Z26(MoAcac), Z26($MoOCl_4$) and Z26(MoO_3)6%He stabilized the four Mo moieties (Fig. S5 and[18]). However, the formation of $[MoO_4]^{2-}$ was inhibited over Z26(MoCO), while Z26($MoCl_5$) stabilized only MoO_3 and $[Mo_2O_7]^{2-}$ moieties[4, 5]. On the other hand, the XRD patterns (Fig. S6) pointed out the presence of an amorphous oxide phase over Z26(MoCO), Z26(MoAcac), Z26($MoCl_5$) and Z26(MoO_3)6%He as the baseline peak at low 2θ values is quite broad, while the pattern of Z26(MoO_3)6%He revealed the diffraction lines of crystalline MoO_3.

The data in Table 4 indicates, additionally, that the concentration of $[Mo_7O_{24}]^{6-}$ species is low. On the other hand, Z26($MoCl_3$) and Z26($MoOCl_4$) presented quasi–similar percentages of MoO_3, $[MoO_4]^{2-}$ and $[Mo_2O_7]^{2-}$ moieties. However, Z26(MoO_3)6%He exhibited low amount of MoO_3 specie, while the percentage of dimeric Mo is identical to that determined for Z26(MoAcac). Interestingly, Z26($MoCl_5$), Z26(MoCO) and Z26($MoOCl_4$) contain quasi–similar amounts of $[Mo_2O_7]^{2-}$ species.

3.2.4 NH_4^+-BEA issued solids

The textural properties and the chemical composition of the solids No XII-XVII are compiled in Table 5.

Table 5. BEA issued solids: Textural and chemical analyses results

Sample	S_{BET}/S_{micro} (m^2g^{-1})	V_p/V_{micro} ($cm^3\ g^{-1}$)	Mo wt. %[a]	Mo wt. loss[b]
NH_4^+–BEA	470/274	0.82/0.13	–	–
BEA($MoCl_3$)	414/267	0.55/0.12	6.14	33
BEA(MoO_3)	540/331	0.59/0.15	5.90	Low
BEA(MoAcac)	460/278	0.55/0.13	6.07	–
BEA(MoCO)	536/325	0.59/0.15	5.09	15
BEA($MoCl_5$)	463/269	0.56/0.12	6.10	–
BEA(Mo_7O_{24})	361/226	0.21/0.10	See Table S8	–
BEA($MoOCl_4$)	–	–	5.15	14

[a] Determined by EDX, [b] $[(Mo_{theoret.} - Mo_{EDX.})/Mo_{theoret.}] \times 100$

The zeolite support possesses a high porous volume, which facilitates the accessibility of $Mo(CO)_6$ toward the internal cavities and reduces, therefore, the Mo wt. loss over BEA(MoCO) solid (15 % vs. 50% for Z26(MoCO)).

The S_{BET} and S_{micro}values do not follow a particular trend. Using Rouquerol conditions (for S_{BET}) and Harkns-Jura equation (for external area), suitable values were obtained with Co/BEA solids[12]. Nevertheless, remarkable values were observed in Table 5; the low S_{BET} and V_p of BEA(Mo_7O_{24}). This outstanding behaviour evidences that most of the Mo introduced occupied the micropores since the metal content determined by EDX is low (Table S8).

The quantification of Mo species by DRS required the determination of the absorption coefficients (K) in Eq. (9). As a matter of fact, we used the areas estimated by the deconvolution of the spectra given in Fig. (4) and the Gauss-Jordan elimination method[22].

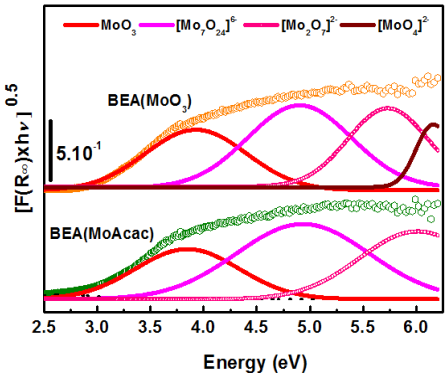

Figure 4. Optical absorption spectra of BEA issued solids. F(R∞) is the Schuster–Kubelka–Munk function, while hν is the photon energy[4,5]

The coefficients were calculated to be $K_{[MoO_4]^{2-}} = 4.97\times10^{-5}$, $K_{[Mo_2O_7]^{2-}} = 4.57\times10^{-5}$, $K_{[Mo_7O_{24}]^{6-}} = 1.90\times10^{-5}$ and $K_{MoO_3} = 1.55\times10^{-4}$ mol g^{-1} $(a.u.)^{-1}$ and the concentrations of different Mo species were collected in Table 6 (see also Table S9).

Table 6 Amount and molar fraction of each Mo moiety over BEA issued solids

Sample	Amount of Mo moieties ($\mu molg^{-1}$) and the corresponding molar fraction (%, value between brackets)				
	$[MoO_4]^{2-}$	$[Mo_2O_7]^{2-}$	$[Mo_7O_{24}]^{6-}$	MoO_3	Mo amount ($molg^{-1}$)
BEA($MoOCl_4$)	101	–	259 (48)	176 (33)	5.36×10^{-4}
BEA(MoO_3)	23	127 (21)	253 (41)	211 (34)	6.14×10^{-4}
BEA($MoCl_5$)	22	145 (23)	317 (50)	151 (24)	6.35×10^{-4}
BEA($MoCl_3$)	60	–	432 (68)	148 (23)	6.40×10^{-4}
BEA(MoAcac)	–	159 (25)	294 (47)	179 (28)	6.32×10^{-4}
BEA(MoCO)	4	134 (25)	216 (41)	176 (33)	5.30×10^{-4}

In Table 6, one can notice that the percentage of $[MoO_4]^{2-}$ species is low. Apparently, during SSIE, monomeric Mo units were condensed either into $[Mo_7O_{24}]^{6-}$ or into $[Mo_2O_7]^{2-}$. Nevertheless, if compared with heptameric Mo, the condensation of monomeric Mo into $[Mo_2O_7]^{2-}$ is less-privileged since BEA($MoOCl_4$) solid still contains $[MoO_4]^{2-}$ (and does not contain dimeric Mo). On the other hand, BEA($MoCl_3$) solid, which theoretically contains 9 wt. % of Mo, stabilizes 68 % of Mo in the form of $[Mo_7O_{24}]^{6-}$ and does not stabilize dimeric Mo despite the fact that it still possesses

monomeric Mo.

For all the samples, the entire condensation of monomeric units during SSIE does not stabilize more than 25% of dimeric Mo and 50% of polymeric Mo. Seemingly, all the used precursors were decomposed during SSIE into MoO_3, which partially transformed into monomeric, dimeric and heptameric species. This is confirmed by the presence of residual MoO_3 in all the samples (Table 6) in amorphous state (see the dashed-square in Fig. S8A). Conversely, MoO_3 exists in crystalline state over BEA(MoO_3) and BEA(Mo_7O_{24}) as revealed within the solid rectangles in Fig. S8B.

The TPR profiles of BEA issued solids and pure MoO_3 are presented in Fig.5.

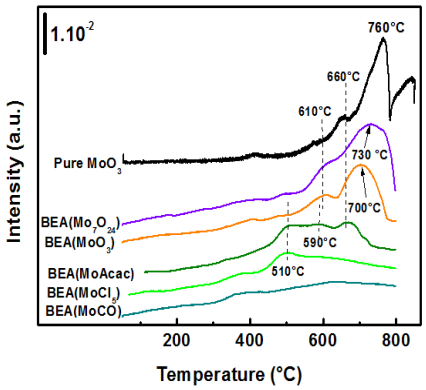

Figure 5. TPR profiles of BEA issued solids and pure MoO_3

The TPR profile of MoO_3 showed two main regions of H_2 consumption. The first region situated below 780°C is related to the reduction of MoO_3 (Eq. 6), while the reduction of MoO_2 (Eq. 7) occurs above 780°C[17, 18, 23]. The TPR profiles of BEA(Mo_7O_{24}) and BEA(MoO_3) showed two peaks at 610 and 720±10°C ascribed to the reduction of crystalline MoO_3 (detected by XRD in Fig. S8B). In effect, the profiles of pure oxide and these two solids exhibit similar shapes. However, the profile of BEA(MoAcac) showed three broad peaks at 510, 590 and 670°C which could be attributed to the reduction of amorphous and crystalline MoO_3. It is worth to note that the profile of BEA(MoCO) does not reveal any reduction peak throughout the investigated temperature range, while for BEA($MoCl_5$) solid we noticed a broad H_2 consumption peak at 510°C due to the reduction of MoO_3.

3.3 Catalytic behaviour of BEA and MFI (26) issued solids: TOF calculations

3.3.1 NH_4^+-ZSM-5 (26) issued solids

Given the fact that $[Mo_2O_7]^{2-}$ was stabilized in all the investigated solids (Table 4), Fig. 6 (A and B) depicts the variation of the $TOF_{[Mo_2O_7]^{2-}}$ values as a function of temperature in ethane and ethylene ammoxidation.

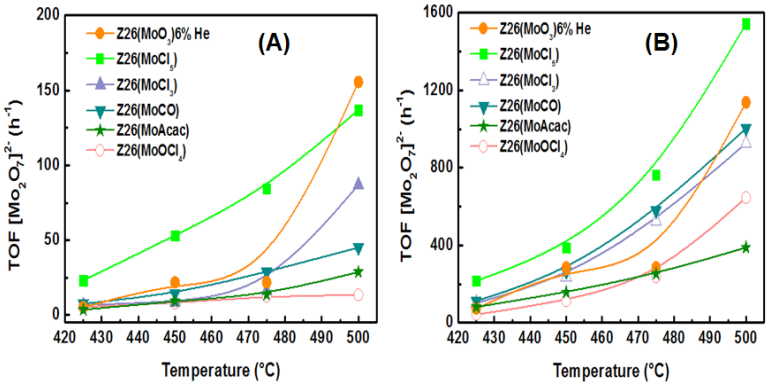

Figure 6. (A) Ethane, and (B) ethylene ammoxidation over ZSM-5 (Si/Al = 26) issued solids: $TOF_{[Mo_2O_7]^{2-}}$ values for acetonitrile activity as a function of reaction temperature (see Tables S10 and S11 for values).

In ethane ammoxidation, Z26($MoCl_5$) catalyst exhibited the highest TOF values between 425-500°C. Nevertheless, Z26(MoO_3)6%He showed the highest value at 500°C. At 500°C, Z26($MoOCl_4$), Z26(MoAcac) and Z26(MoCO) had turnover frequency values that did not exceed 50 h^{-1}, while Z26($MoCl_3$) offered an intermediate value (~75 h^{-1}).

In ethylene ammoxidation, Z26($MoCl_5$) presented the highest TOF values regardless of the reaction temperature. However, the lowest values were obtained over Z26($MoOCl_4$) and Z26(MoAcac), while Z26(MoO_3), Z26(MoCO) and Z26($MoCl_3$) showed intermediate values.

It is important to note that Z26(MoO_3)6%He catalyst exhibited a singular behaviour in ethane ammoxidation at 500°C (highest TOF value). In order to understand such behaviour, we performed XPS analyses after ethane ammoxidation (Fig.7, where we also included the spectrum of the poorly active Z26(MoAcac) catalyst).

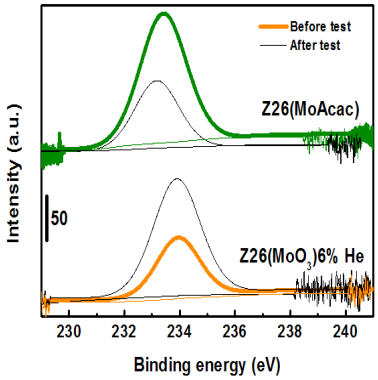

Figure 7. XP spectra of Z26(MoO_3)6%He and Z26(MoAcac) catalysts before and after ethane ammoxidation: Mo3d5/2 component ascribed to bulky MoO_3

According to Fig. 7, there is an enrichment of Z26(MoO_3)6%He catalyst's surface with MoO_3 after catalytic test. On the contrary, the reversed trend is observed in the case of Mo(MoAcac) catalyst, i.e. MoO_3 oxide migrates throughout the internal cavities of the zeolite.

3.3.2 NH_4^+-BEA issued solids

Fig. 8 (A and B) represents the variation of $TOF_{[Mo_2O_7]^{2-}}$ values as a function of temperature.

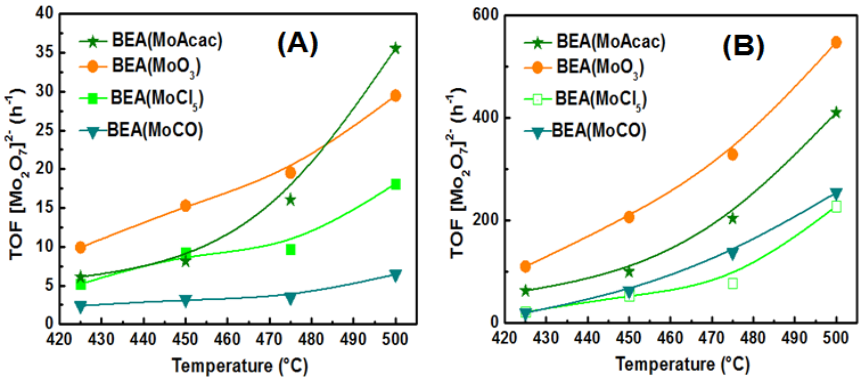

Figure 8. (A) Ethane, and (B) ethylene ammoxidation over BEA issued solids: $TOF_{[Mo_2O_7]^{2-}}$ values for acetonitrile activity as a function of reaction temperature (see Tables S10 and S11 for values)

In the studied reactions, BEA($MoCl_5$) and BEA(MoCO) are poorly active catalysts. However, BEA(MoO_3) exhibited the highest TOF values between 425 and 500°C. Nevertheless, if compared with BEA($MoCl_5$), BEA(MoAcac) catalyst exhibited higher turnover frequency values between 450 and 500°C in ethane ammoxidation.

3.3.3 $MoOCl_4$ issued solids

BEA($MoOCl_4$) solid does not contain dimeric Mo but has $[Mo_7O_{24}]^{6-}$ species which do not catalyze the ammoxidation reaction (check the behaviour of the poorly active BEA($MoCl_3$) catalyst despite containing higher amounts of $[Mo_7O_{24}]^{6-}$ species). On the other hand, Z26($MoOCl_4$) contains dimeric Mo and low amounts of $[Mo_7O_{24}]^{6-}$ species. Both catalysts contain monomeric Mo and exhibit similar catalytic properties (Tables S1 and S2). Bearing this in mind, the TOF values

relative to $[MoO_4]^{2-}$ species over BEA($MoOCl_4$) and Z26($MoOCl_4$) were calculated and compiled in Fig.S10.

According to Fig. S10 (A and B), BEA($MoOCl_4$) catalyst exhibited higher TOF values if compared with Z26($MoOCl_4$).

4. Discussion

4.1 OFF and FER issued catalysts

The treatment of Mo chlorides and zeolites during the SSIE would result in the formation of cationic species like $[Mo_2Cl_2]^{4+}$ and $[MoCl]^{2+}$ instead of bare Mo^{3+}[24]. In the OFF framework, six different oxygen atoms have been numbered (Scheme S1[25]). O_5 atom, located in the channels and in gmelinite cages (aperture 5 Å), is largely accessible to hydrocarbons and NH_3, while O_2 and O_4, located in cancrinite cages (aperture 1.8 Å), are less accessible to hydrocarbons but interact with NH_3. Nevertheless, O_6 atom is located in hexagonal prisms, which are inaccessible to NH_3[25].

In the studied reactions, Mo-OFF catalyst is poorly active. Ethane (kinetic diameter d = 4.44 Å[11]), ethylene (d = 4.00 Å[11]), dioxygen (d = 3.46 Å[15]) and NH_3 (d = 2.90 Å[26]) molecules are accessible only to the main channels and gmelinite cages of offretite. Nevertheless, CH_3CN (d = 4.97 Å[11]) produced during ammoxidation would be trapped inside the gmelinite cages and then oxidized into CO_2 (selectivity toward $CO_2 \geq 92\%$). The hydrocarbon(s) molecules (reactants or intermediate), which have no access to the hexagonal prisms and cancrinite cages, will be oxidized over amorphous MoO_3 (E_g = 3.00 eV in Fig. 3, vs. 2.88 eV[18] for commercial MoO_3).

Ferrierite is a medium-pore sized zeolite containing a bi-dimensional pore system consisting of 10 membered ring (MR) channels (4.3×5.5 Å) and 8 MR channels (3.5×4.8 Å)[27,28]. The interaction between molecules having permanent moment (e.g. N_2) and the electric field of ferrierite is weak, which explains the failure of our textural analysis. At the contrary, polar H2O molecules, strongly interacted with the electric field, would inhibit the entire dehydration of the ferrierite.

Under the SSIE conditions employed, the humid ferrierite sample would evolve H_2O toward $MoCl_3$ below 450°C[29]. As a matter of fact, the hygroscopic $MoCl_3$ will be readily transformed into $MoOCl_{2x(g)}$ (x = 1, 1.5 or 2) leading to a significant Mo weight loss. Furthermore, residual $MoOCl_{2x(g)}$ could be transformed into MoO_3 (Eq. 10) as we proposed for $MoCl_5$[24].

$$MoOCl_{2x(g)} + 2H_2O_{(g)} \rightarrow MoO_{3(s)} + 2xHCl_{(g)} + (2-x)H_{2(g)} \quad (10)$$

Apparently, the reaction in Eq. (10) is displaced toward the right side since the XP spectrum of Mo-FER solid revealed the presence of, only, MoO_3 at the surface. Such oxide, which hinders the surface silanol groups (see the decrease in the 3735 cm^{-1} band's intensity in Fig. 3A), exists in a crystalline state reduced under H_2 at 550 and 630°C.

Despite the presence of crystalline MoO_3, which catalyzes the reaction in Eq. (2), Mo–FER catalyst is inactive in ethane ammoxidation. Apparently, the oxide particles sited at the catalyst's surface blocked the zeolite channels and inhibited the diffusion of C_2H_6 toward the internal active sites. As for the ethylene ammoxidation, the structure of this catalyst does not permit effective mixing of reactants as the totality of Mo occupied the surface.

4.2. MoCl3 issued catalysts

Upon the SSIE, the small 8 MR side-pockets (2.6×5.7 Å) in mordenite[19] favoured the formation of amorphous MoO3 agglomerates[19], while DRS results revealed the presence of $[MoO_4]^{2-}$ and $[Mo_7O_{24}]^{6-}$ species. In ethane ammoxidation, MOR($MoCl_3$) is the least active catalyst since amorphous MoO_3 catalyzes the secondary reaction and inhibits the accessibility of reactants toward internal active sites. However, in ethylene ammoxidation, this catalyst exhibited an interesting behaviour due to the presence of medium–strength acid sites[19], which easily desorbed NH3 required in Eq.(3). In fact, strong acid–sites are inefficient in acid catalysis over mordenite[30].

The BEA issued solid exhibited superior activity if compared with MOR($MoCl_3$). This behaviour would be ascribed to the nature of oxide phase stabilized within BEA($MoCl_3$). In effect, the XRD and TEM analyses reported in ref.[19] indicated the presence of small aggregates of crystalline MoO_3. The obstruction of the BEA channels is, therefore, excluded.

The SSIE of $MoCl_3$ into MFI zeolites (Si/Al = 15 and 26) stabilizes, besides MoO_3, monomeric and dimeric Mo. However, $[Mo_7O_{24}]^{6-}$ species were detected over Z15($MoCl_3$) solid, only, due to the availability of neighbouring Al atoms in this Al–rich zeolite (2.44 wt. %[19]). In catalysis, Z15($MoCl_3$) and Z26($MoCl_3$) exhibited remarkable activities due to the presence of $[Mo_2O_7]^{2-}$ species considered as potential active sites. Nevertheless, higher CO_2 selectivity was recorded over Z15($MoCl_3$) due to the fact that Mo species are in deep interaction with the highly-charged ZSM-5 (Si/Al = 15) framework as they were hardly reduced under H_2 (see TPR results in[19]). During the SSIE, H_2O should be evolved easily in order to

transform $MoCl_3$ into $MoOCl_{2x}$ and then into MoO_3, required to form the exchangeable $MoO_2(OH)_2$ species (Eq. 11).

$$MoO_{3(s)} + H_2O_{(g)} = MoO_2(OH)_{2(s)} = MoO_2(OH)_{2(g)} \quad (11)$$

Nevertheless, if the zeolite is hardly dehydrated, MoO_3 does not transform adequately into $MoO_2(OH)_{2(g)}$ during SSIE but rather undergoes agglomeration at the catalyst's surface and blocks the channels during ammoxidation and/or enhances the hydrocarbons oxidation.

The exchange of ZSM-5 zeolite ($\Delta_{dehyd.}H$ = 7.60 k*J* mol^{-1}) with $MoCl_3$ would stabilize less amounts of MoO_3 than that of BEA ($\Delta_{dehyd.}H$ = 13.94 k*J* mol-1) exchanged with the same precursor (respectively 115 and 148 $\mu molg^{-1}$ of MoO_3). Therefore, during the exchange of $MoCl_3$ into BEA, the precursor is transformed into MoO_3 (Eq. 10). This oxide is then transformed into $[MoO_4]^{2-}$ (Eq. 12) which further undergoes two possible transformations (Eqs. 13 and 14).

$$MoO_3 \rightarrow MoO_2(OH)_2 \rightarrow [MoO_4]^{2-} \quad (12)$$

$$[MoO_4]^{2-} \rightarrow [Mo_2O_7]^{2-} \quad (13)$$

$$[MoO_4]^{2-} \rightarrow [Mo_7O_{24}]^{6-} \quad (14)$$

Over Z26($MoCl_3$) solid, only reactions (10), (12) and (13) occur since no $[Mo_7O_{24}]^{6-}$ species were formed. However, in the case of BEA($MoCl_3$), only reactions (10), (12) and (14) take place. Seemingly, the condensation of monomeric Mo into $[Mo_7O_{24}]^{6-}$ over an Al-poor zeolite, i.e. ZSM-5 (Si/Al = 26, 1.30 wt. % of Al vs. 2.77 for BEA[19]), is disfavoured.

In catalysis, BEA($MoCl_3$) is a poorly active solid although it contains 432 $\mu molg^{-1}$ of $[Mo_7O_{24}]^{6-}$ species, whereas, the superiority of Z26($MoCl_3$) catalyst is attributed to the presence of 53 $\mu molg^{-1}$ of $[Mo_2O_7]^{2-}$ species.

4.3 $MoOCl_4$ and $MoCl_5$ issued catalysts

BEA($MoOCl_4$) solid loaded, apart from monomeric Mo, higher amounts of MoO_3 (176 $\mu mol\ g^{-1}$) and $[Mo_7O_{24}]^{6-}$ (259 $\mu mol\ g^{-1}$), i.e. only reactions in Eqs. (10), (12) and (14) occur). However, the solid issued from ZSM-5 (Si/Al = 26) stabilized very high amounts of monomeric Mo (340 $\mu molg^{-1}$) and dimeric Mo (80 $\mu molg^{-1}$), i.e. reactions (12) and (13) are predominant.

In catalysis, $[MoO_4]^{2-}$ species catalyze ethane dehydrogenation[31] and activate ammonia molecules required for ammoxidation[3]. Nevertheless, the variation of TOF relative to monomeric Mo revealed that Z26($MoOCl_4$) is the least active catalyst despite the presence of dimeric Mo. In order to understand this controversy, we performed SEM analysis with the intention of verifying the morphology of BEA($MoOCl_4$) and Z26($MoOCl_4$) solids (Fig. 9).

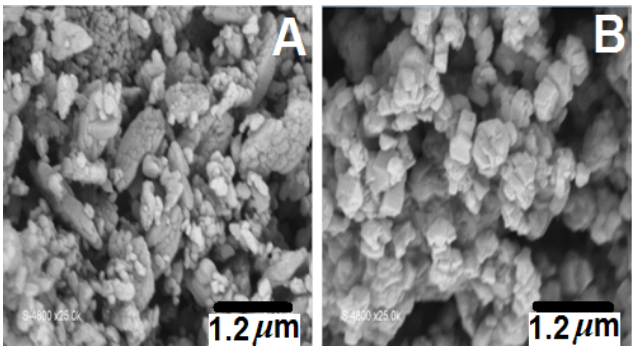

Figure 9. SEM micrograph of (A) BEA($MoOCl_4$), and (B) Z26($MoOCl_4$) solids

Fig. 9B showed that Z26($MoOCl_4$) contains mainly spherical agglomerates of zeolite particles, while the grains of BEA($MoOCl_4$) sample are less-interconnected with a size below 1.2 μm. Such an agglomeration over Z26($MoOCl_4$) has a negative effect in ammoxidation despite the presence of dimeric Mo. In this context, Batalha et *al*.[32] reported that the diffusion of butane into BEA zeolite increases with the decrease in aggregates' size[32].

The inversed trend is observed with $MoCl_5$ issued solids. In effect, Z26($MoCl_5$) catalyst exhibited the highest activity, while BEA($MoCl_5$) is poorly active. Both solids contain dimeric Mo and a similar concentration of MoO_3 reduced at the temperature (510°C in Fig. 5 and 515°C in[4]). This behaviour cannot be ascribed to the obstruction of the BEA channels by

oxide since all the BEA issued solids exhibited a significant decrease in porosity. On the other hand, both solids contained amorphous oxide (dashed-squares in Figs. S6 and S8A).

We analyzed Z26($MoCl_5$) and BEA($MoCl_5$) solids by SEM (Fig.10).

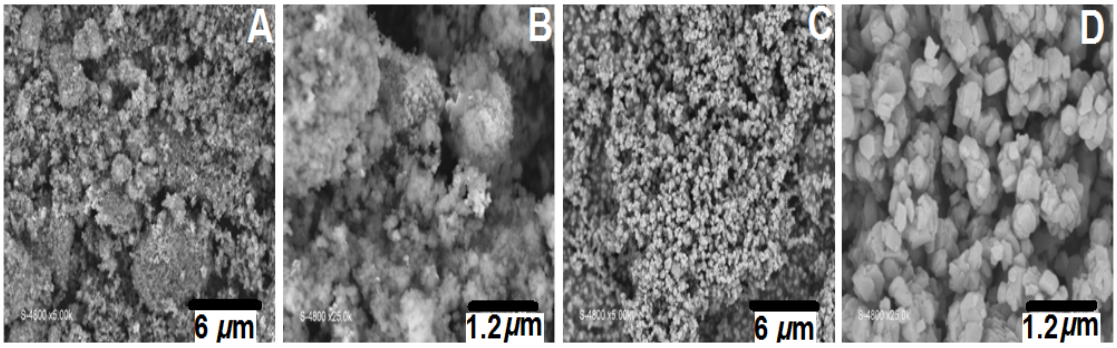

Figure 10. SEM micrographs of (A) and (B) BEA($MoCl_5$), and (C) and (D) Z26($MoCl_5$) solids

The micrographs revealed the aggregation of zeolite particles over BEA($MoCl_5$) solid. Similarly to Z26($MoOCl_4$) solid, the aggregation of the particles would inhibit the ammoxidation reactants to reach internal active sites of BEA($MoCl_5$) catalyst, namely monomeric and dimeric Mo species (respectively 22 and 145 $\mu molg^{-1}$).

4.4 Interpretation of TOF values

In ethylene ammoxidation, dimeric Mo over Z26(MoCO) and Z26($MoCl_3$) catalysts led to quasi-similar TOF values. However, in ethane ammoxidation, Eq. (2) was successfully catalyzed by monomeric Mo over Z26($MoCl_3$) catalyst (344 $\mu molg^{-1}$), which explains the higher TOF value obtained at 500°C if compared with that of Z26(MoCO). The contribution of crystalline MoO_3 in ethane ammoxidation over these two catalysts is not clear since their DRS spectra revealed a similar E_g (MoO_3) value (2.96 eV). As for BEA(MoCO) and BEA($MoCl_5$), similar TOF values were obtained in ethylene ammoxidation. This behaviour is expected as these two solids loaded dimeric Mo at quasi–comparable concentrations. However, in ethane ammoxidation, we can notice (in Fig. 8A) the higher TOF values obtained with BEA($MoCl_5$) due to the contribution of monomeric Mo (22 $\mu molg^{-1}$) in the reaction illustrated in Eq. (2). Moreover, the contribution of crystalline MoO^3 in Eq. (2) cannot be neglected over BEA(MoCO) due to the higher C_2H_4 activity obtained without the contribution of monomeric Mo (~4 $\mu molg^{-1}$). Apparently, crystalline MoO_3 exists in a highly dispersed state over BEA(MoCO) since no TPR features were observed in Fig. 5. However, over BEA($MoCl_5$) catalyst, amorphous MoO_3 catalyzed the secondary reaction in ethylene and ethane ammoxidation at 500°C. Herein, we can attribute the peak at 510°C in the TPR profile of BEA($MoCl_5$) solid to amorphous MoO_3.

Over Z26(MoO_3)6%He catalyst, the TOF values are insignificant between 425 and 450°C despite the presence of large crystallites of MoO_3 which inhibit the diffusion of reactants toward active sites (i.e. 28 $\mu molg^{-1}$ of dimeric Mo). Nevertheless, at 500°C, the highest TOF value was obtained. Apparently, increasing the temperature and the presence of oxygen as an ammoxidation reactant improved the dispersion state of crystalline MoO_3 which catalyzes the reaction in Eq.(2) namely at 500°C. This hypothesis has been confirmed by the XRD pattern of Z26(MoO_3)6%O_2 in Fig. S10, which revealed the decrease in the intensity of MoO_3 diffraction lines. On the other hand, the XPS analyses performed before and after catalytic tests indicate that MoO_3 migrates from the internal cavities of Z26(MoO_3)6%He catalyst toward the surface. The inversed trend was observed over Z26(MoAcac) which exhibited very low TOF values.

The exchange of $MoO_2(C_5H_7O_2)_2$ into ZSM-5 (Si/Al = 26) favoured the agglomeration of amorphous MoO_3 which diffuses inside the channels during test and inhibits the accessibility of reactants toward the 418 $\mu molg^{-1}$ of $[MoO_4]^{2-}$ and the $\mu molg^{-1}$ of $[Mo_2O_7]^{2-}$ active species[3, 33].

The exchange of MoO_3 into BEA zeolite led to an active catalyst. In effect, BEA(MoO_3) solid contains crystalline MoO_3, monomeric Mo (23 $\mu molg^{-1}$) and $[Mo_2O_7]^{2-}$ (12 $\mu molg^{-1}$) species. On the other hand, we noticed a linear increase in the TOF values between 425 and 500°C, which points out that the dispersion state of crystalline MoO_3 over BEA(MoO_3) catalyst is kept intact during catalytic tests. Nevertheless, in the case of BEA(MoAcac), TOF values increase at high temperatures due to the improvement in the dispersion state of crystalline MoO_3 (reducible under H_2 at 590 and 660°C). At low temperatures, TOF values are low since BEA(MoAcac) does not contains monomeric Mo, while MoO_3 is present in the amorphous state (reducible under H_2 at 510°C).

The contribution of crystalline MoO_3 in ethane oxidative dehydrogenation depended on its dispersion state. In this

context, crystalline MoO_3 over BEA(Mo_7O_{24}) solid (detected by XRD) was reduced under H_2 at high temperatures (730°C vs. 700°C for BEA(MoO_3) solid). Apparently, this oxide phase occupied the internal micropores due to the significant decrease in the SBET and the porosity of the support (see the table p. S13) and to the low concentrations of Mo at the surface. In ethane ammoxidation, BEA(Mo_7O_{24}) catalyst exhibited lower catalytic activity if compared with BEA(MoO_3). This behaviour is due to the presence of crystalline MoO_3 inside the micropores; such an oxide phase is inefficient in ammoxidation as also revealed over Z26(MoAcac) catalyst.

4.5 Reference catalysts

Starting from ZSM-5 (Si/Al = 26) and MoO_3, very high Mo amount (10 wt. %) improved the catalytic activity in ethylene ammoxidation at 500°C (26.50 $\mu mols^{-1}g^{-1}$ over Z26(MoO_3)10%He vs. 8.90 $\mu mols^{-1}g^{-1}$ for Z26(MoO_3)6%He). Apparently, the excess of Mo stabilizes higher amounts of mono– and dimeric active species (by analogy with Z26(MoO_3)6%He) as well as crystalline MoO_3. Nevertheless, the exchange of 6 wt. % of Mo over ZSM-5 (Si/Al = 140) led to low AN activity in C_2H_4 ammoxidation at 500°C (5.60 $\mu mols^{-1}g^{-1}$ over Z140(MoO_3)6%He vs. 8.90 $\mu mols^{-1}g^{-1}$ over Z26(MoO_3)6%He). Due to the very high Si/Al ratio (and very low $\Delta_{dehyd.}H$), ZSM-5 zeolite (Si/Al =140) seems hydrophobic and, therefore, the transformation of MoO_3 into $MoO_2(OH)_2$ (Eq. 11) and then into active species (via Eqs. 12 and 13) does not take place. In effect, the textural properties of Z140(MoO_3)6%He and Z140(MoO_3)6%O_2 (page S13) are quite-similar, evidencing that MoO_3 does not diffuse inside the channels in the absence of H_2O.

The humid impregnation of a hydrophobic zeolite (ZSM-5, Si/Al = 40) with MoO_3 at 2 and 4 wt. % of Mo (Z40(MoO_3) Imp2% and Z40(MoO_3)Imp4%, respectively) led to 15.50 and 18 $\mu mols^{-1}g^{-1}$ of AN activity. These catalytic activities exceed those obtained with the highly hydrophobic ZSM-5 (Si/Al =140) despite the use of low Mo wt. %. This behaviour is due to the fact that ZSM-5 (Si/Al = 40) retained H_2O molecules during the impregnation which favours the formation of $MoO_2(OH)_2$ (Eq. 11) and the stabilization of active species (Eqs. 12 and 13). The impregnation of 4 wt. % of Mo into a hydrophilic zeolite (ZSM-5, Si/Al =15), i.e. Z15(MoO_3)Imp4% solid, led to the highest activity (29.70 $\mu mols^{-1}g^{-1}$ of AN activity at 500°C vs. 17.80 $\mu mols^{-1}g^{-1}$ over Z40(MoO_3)Imp4%). In particular, 4 wt. % of Mo exchanged with hydrophobic or hydrophilic zeolite led to very high AN selectivity at low temperatures. Apparently, in a water–rich atmosphere, 2 wt. % of Mo are inefficient to produce enough active species from MoO_3 since the textural properties of Z15(MoO_3)Imp2% and ZSM-5 zeolite (Si/Al =15) are similar (page S13), i.e. there is no residual MoO_3 able to clog the zeolite channels.

5. Conclusion

We studied the light hydrocarbons conversion into acetonitrile over Mo exchanged zeolites. In ethylene ammoxidation, the most active catalysts are those prepared by the humid impregnation of MoO_3 (4 wt. %) into MFI zeolite, having low dehydration enthalpy $\Delta_{dehyd.}H$ (11.70 k*J*mol^{-1}, Si/Al ratio = 15). Nevertheless, increasing Si/Al ratio from 15 to 40 or decreasing the metal amount from 4 to 2 wt. % decreased the selectivity toward the desired product. On the other hand, the exchange of high amount of MoO_3 (10 wt. %) by solid–state ion exchange method is suitable but the use of hydrophobic zeolites (very high Si/Al ratios, i.e. 140) should be avoided. In effect, water molecules are required to transform MoO_3 into the exchangeable $MoO_2(OH)_2$ species. Starting from NH_4^+-BEA (Si/Al = 12.21, $\Delta_{dehyd.}H$ = 13.94 k*J*mol^{-1}) and NH_4^+-ZSM-5 zeolite (Si/Al = 26, $\Delta_{dehyd.}H$ = 7.60 k*J*mol-*1*) and using MoO_3 precursor, the corresponding catalysts are very active at high temperatures (500°C) due to the stabilization of crystalline MoO_3. In ethane and ethylene ammoxidation, $[MoO_4]^{2-}$, $[Mo_2O_7]^{2-}$ and crystalline MoO_3 are the active species. However, due to their particular structures and higher dehydration enthalpy values, FER, OFF and MOR zeolites do not allow the stabilization of these species. Furthermore, $MoOCl_4$, $Mo(CO)_6$, $MoCl_3$ should be avoided as they stabilize inefficient $[Mo_7O_{24}]^{6-}$ species and amorphous MoO_3. By choosing the adequate precursors ($MoCl_5$, $MoO_2(C_5H_7O_2)_2$ and MoO_3) the dehydration state of the zeolite (i.e. $\Delta_{dehyd.}H$ and Si/Al values) would be taken in consideration.

Acknowledgement

Emna Mannei and Faouzi Ayari:

We would like to thank Pr. Zouhaier Ksibi for giving us the opportunity to perform scientific research in the Material chemistry and catalysis laboratory.

This article contains supplementary information online at:
http://ojs.wiserpub.com/index.php/FCE/article/view/117/115

Conflict of interest

The authors declare no competing financial interest.

References

[1] Neal L, Haribal V, McCaig J *et al*. Modular-scale ethane to liquids via chemical looping oxidative dehydrogenation: Redox catalyst performance and process analysis. *J Adv Manuf Process.* 2019; 1: 1-8.

[2] Gue E. Midstream MLPs: The best way to ride the U.S. petrochemical wave. *Seeking Alpha.* Available from: https://seekingalpha.com/article/4042473-midstream-mlps-best-way-ride-u-s-petrochemical-wave. [Accessed 27th, June 2017].

[3] Mannei E, Ayari F, Petitto C *et al*. Light hydrocarbons ammoxidation into acetonitrile over Mo-ZSM-5 catalysts: Effect of molybdenum precursor. *Microporous Mesoporous Mater*. 2017; 241: 246-257.

[4] Mannei E, Ayari F, Asedegbega-Nieto E *et al*. Physicochemical and catalytic properties of over- and low-exchanged Mo–ZSM-5 ammoxidation catalysts. *Chem Papers.* 2019; 73: 619-633.

[5] Mannei E, Ayari F, Asedegbega-Nieto E *et al*. Catalytic behaviour of molybdenum-based zeolitic materials prepared by organic-medium impregnation and sublimation methods. *J. Iran. Chem. Soc.* 2019. Available from: https://doi.org/10.1007/s13738-019-01837-6.

[6] Li Y, Armor JN. Ammoxidation of ethane to acetonitrile over metal-zeolite catalysts. *J Catal.* 1998; 173: 511-518.

[7] Jeong Y-S, An SH and Shin C-H. Selective synthesis of acetonitrile by reaction of ethanol with ammonia over Ni/Al2O3 catalyst. *Korean J Chem Eng.* 2019; 36: 1051-1056.

[8] Boschloo G, Hagfeldt A. Characteristics of the iodide/triiodide redox mediator in dye-sensitized solar cells. *Acc Chem Res.* 2009; 42: 1819-1826.

[9] Partington JR, Cowley EG. Dipole moment of acetonitrile. *Nature.* 1935; 135: 474.

[10] *The Phamraceutical Journal*, Acetonitrile shortage. Available from: https://www.pharmaceutical-journal.com/news-and-analysis/acetonitrile-shortage/10047706.article?firstPass=false. [Accessed 29th, January 2009]

[11] Essid S, Ayari F, Bulánek R *et al*. Over- and low-exchanged Co/BEA catalysts: General characterization and catalytic behaviour in ethane ammoxidation. *Catal Today*. 2018; 304: 103-111.

[12] Essid S, Ayari F, Bulánek R *et al*. Improvement of the conventional preparation methods in Co/BEA zeolites: Characterization and ethane ammoxidation. *Solid State Sci.* 2019; 93: 13-23.

[13] Mitchell PCH. Molybdenum in enzymatic and heterogeneous catalysis. *J Inorg Biochem.* 1986; 28: 107-123.

[14] Ferdjaoui NH, El Berrichi FZ and Ayari F. Kaolin-issued zeolite A as efficient adsorbent for Bezanyl Yellow and Nylomine Green anionic dyes. *Microporous Mesoporous Mater.* 2017; 243: 91-101.

[15] Breck DW, Grose RW. A Correlation of the calculated intracrystalline void volumes and limiting adsorption volumes in zeolites. In: Molecular Sieves. *Advances in Chemistry*. ACS Washington DC; 1973. p. 319-329.

[16] Kosinov N, Coumans FJAG, Uslamin E *et al*. Selective coke combustion by oxygen pulsing during Mo/ZSM-5-catalyzed methane dehydroaromatization. *Angew Chem.* 2016; 128: 15310-15314.

[17] Arnoldy P, de Jonge JCM and Moulijn JA. Temperature-programmed reduction of MoO_3 and MoO_2. *J Phys Chem.* 1985; 89: 4517-4526.

[18] Ayari F, Mannei E, Asedegbega-Nieto E *et al*. More insight on the isothermal spreading of solid MoO_3 into ZSM-5 zeolite. *React Kin, Mech Catal.* 2018; 124: 419-436.

[19] Mannei E, Ayari F, Mhamdi M *et al*. Ammoxidation of C_2 hydrocarbons over Mo-zeolite catalysts prepared by solid-state ion exchange: Nature of molybdenum species. *Microporous Mesoporous Mater*. 2016; 219: 77-86.

[20] Vieillard P, Mathieu R. A predictive model for the enthalpies of hydration of zeolites. *Amer Miner.* 2009; 94: 565-577.

[21] Djajanti SD, Howe RF. MOCVD in zeolites using $Mo(CO)_6$ and $W(CO)_6$ as precursors. *Stud Surf Sci Catal*. 1995; 97: 197-204.

[22] Mon Y, Win Kyi L. Performance comparison of Gauss elimination and Gauss-Jordan elimination. *Int J Comput Commun Eng Res*. 2014; 2: 67-71.

[23] Bhaskar T, Reddy KR, Kumar CP *et al*. Characterization and reactivity of molybdenum oxide catalysts supported on zirconia. *Appl Catal A: Gen.* 2001; 211: 189-201.

[24] Ayari F, Mannei E, Asedegbega-Nieto E *et al*. Elucidation of the solid-state ion exchange mechanism of $MoCl_5$ into ZSM-5 zeolite. *Thermochim Acta.* 2017; 655: 269-277.

[25] Mirodatos C, Abou-Kais A, Vedrine JC *et al*. Characterization of the hydroxyls in offretite zeolite. J Chem *Soc, Faraday Trans.* 1978; 74: 1786-1795.

[26] Zhang R, Liu N, Lei Z *et al*. Selective transformation of various nitrogen–containing exhaust gases toward N2 over zeolite catalysts. *Chem Rev.* 2016; 116: 3658-3721.

[27] Hu H, Ke M, Zhang K *et al*. Designing ferrierite–based catalysts with improved properties for skeletal isomerization of n-butene to isobutene. *RSC Adv*. 2017; 7: 31535-31543.
[28] Kerr IS. Structure of ferrierite. *Nature*. 1966; 210: 294-295.
[29] Verbiest J,Vansant EE. Dehydration, deammoniation and thermal stability of ferrierite. *Bull Soc Chim Belq.* 1986; 95: 75-81.
[30] Miwa M, Suzuki K, Katada N *et al*. Ammonia IRMS-TPD study on the distribution of acid sites in mordenite. J Phys Chem B. 2005; 109: 18749-18757.
[31] Hadded N, Bordes-Richard E, Hilaire L *et al*. MoOx-based catalysts for the oxidative dehydrogenation (ODH) of ethane to ethylene: Influence of vanadium and phosphorus on physicochemical and catalytic properties. *Catal Today.* 2007; 126: 256-263.
[32] Batalha N, Soualah A, Pinard L *et al*. Impact of the BEA zeolite morphology on isobutane adsorption followed by reversed-flow inverse gas chromatography. J Chromatogr A. 2012; 1260: 206-214.
[33] Ayari F, Mannei E, Asedegbega-Nieto E *et al*. Solid-state ion exchange of molybdenum (VI) acetylacetonate into ZSM-5 zeolite. *Thermochim Acta*. 2017; 652: 150-159.